May 2021

Considerations for Testing Full-Scale Wind Turbine Nacelles with Hardware-in-the-Loop

Kirk Christopher Heinold
Clemson University, kcheinold@gmail.com

Considerations for Testing Full-Scale Wind Turbine Nacelles with Hardware-In-the-Loop

---

A Thesis
Presented to
the Graduate School of
Clemson University

In Partial Fulfillment
of the Requirements for the Degree
Master of Science
Mechanical Engineering

---

by
Kirk C. Heinold
May 2021

Accepted by:
Dr. Richard Figliola, Committee Chair
Dr. Amin Bibo
Dr. Gang Li
Dr. Meghashyam Panyam

Abstract

Full-scale wind turbine nacelle testing with Hardware-In-the-Loop (HIL) configuration allows full operational certification testing with native nacelle controllers, as opposed to open-loop testing which requires significant modification of the controller to bypass missing subsystems when the nacelle is mounted on the test bench. Implementation of Hardware-In-the-Loop testing involves running a real-time simulation of a full turbine model in parallel with the test bench in order to account for the missing rotor, tower, platform, and actuators. For successful implementation of this method, first, the simulation model should be able to capture the dynamic characteristics of the turbine accurately while also meeting the real-time requirements. Second, the deviations resulting from the different boundary conditions between the drivetrain in a full turbine and the test bench environment should be mitigated. In the first part of the study, a sensitivity analysis is performed using a baseline wind turbine model to determine the minimum drivetrain fidelity level necessary to capture the dynamics with a focus on the torsional characteristics that are crucial for performing electro-mechanical certification tests. The results show that the torsional dynamics are dominated by the flexibility of the main shaft and the gearbox supports. The rest of the components can be significantly simplified thereby reducing the total number of modes and degrees of freedom for real-time execution.

In the second part of the study, the reduced drivetrain model is utilized in a comparative analysis to quantify the deviations in torsional dynamics resulting from the rigid connections and test bench components (motor, reduction gearbox, and the load application unit) replacing the tower and rotor, respectively. It is found that the different mechanical interfaces can shift the first torsional mode of the drivetrain by as much as 19% which can significantly impact electro-mechanical responses. The feasibility of exploiting the test bench speed controller to introduce virtual inertia, damping, and stiffness and compensating for such differences is studied. It is demonstrated that

the controller can be tuned to perform pole placement and match the torsional frequencies between the coupled test bench-nacelle and the full turbine. Finally, the performance of the tuned controller is verified using two case studies: a) free response to characterize the torsional responses in a low voltage ride through scenario, and b) forced response to evaluate its ability to track a highly dynamic speed profile resulting from a turbulent wind profile.

Table of Contents

List of Tables

List of Figures

Chapter 1

Introduction

Many countries worldwide are using less fossil fuels and increasingly rely on renewable energy sources for power generation, including wind energy. The global wind energy installation increased by 17% in 2019 alone, bringing the global capacity to 650 GW [1]. Vast wind resources exist globally and in the United States for future expansion of wind farms, including in many locations offshore along the East and West coast, near large population centers. However, efforts must be continued to reduce the cost of wind energy to ensure the growth of wind in the future.

Reliability of drivetrain components within the nacelle makes a large contribution to the operation and maintenance costs of wind turbines, which are significant relative to most traditional energy sources. Evaluation of wind turbine component reliability through testing is one area that can be used to lower the maintenance cost [2], and avoid blackouts due to shutdown, making wind energy more economical. The term nacelle refers to the housing at the top of the tower of a wind turbine and all the drivetrain components inside of it including the main shaft, main bearing, bedplate, gearbox, high-speed coupling, generator, and the yaw interface. Previously, testing relied on individual components, such as the gearbox [3], generator [4], and controller [5]. However, studies have suggested that these tests do not necessarily emulate the realistic mechanical loads on the components as a system [6]. Wind turbine nacelle test benches equipped with electric grid simulators are currently the most comprehensive testing strategy that captures the electro-mechanical response of nacelle components under load.

1.1 Wind Turbine Nacelle Test Benches

Wind turbine nacelle test laboratories provide a controlled environment to evaluate responses of full-scale drivetrains when subjected to mechanical and/or electrical loads and conditions that they would otherwise experience in the field. A few facilities around the world have the equipment to perform such testing. These facilities typically include dynamometers that comprise of a drive motor and a Load Application Unit (LAU) to apply torque and non-torque loads for mechanical testing. For electrical testing, they are equipped with grid simulators that couple with the generator with-in the nacelle for emulating electrical loads/grid conditions. Among these facilities, the Clemson University WTDTF located in Charleston, SC, houses two test benches capable of testing wind turbine drivetrains with capacities up to 7.5 MW and 15 MW, respectively. Fig. 1.1 shows an image of the 7.5 MW test bench at the Clemson WTDTF.

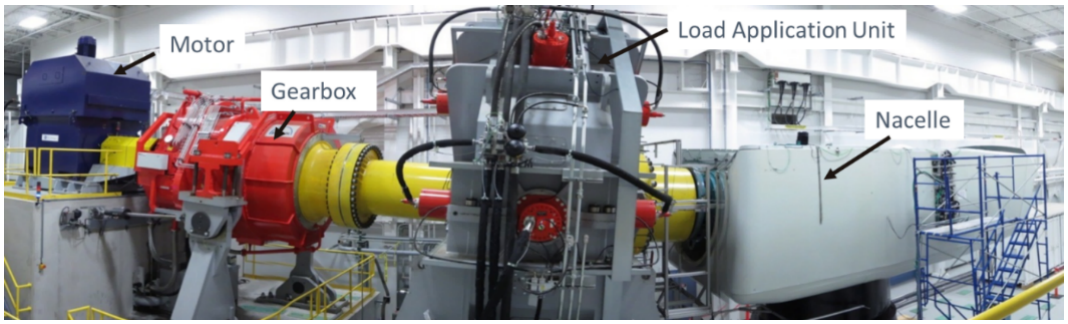

Figure 1.1: Clemson University's 7.5 MW Test Bench

The asynchronous drive motor on this test bench is coupled to the LAU through a high-speed coupling and a reduction gearbox. The LAU consists of a disk and hydraulic actuator assembly which enables it to apply non-torque loads at the main shaft of the nacelle while spinning. During testing, the test bench controller issues the speed command to the drive motor, the commanded load vector to the LAU, and the generator torque command through the nacelle controller. Those signals can be applied either statically or dynamically depending on the test objective.

The mechanical loads applied to the nacelle typically encompass the Design Load Cases (DLCs) prescribed in the IEC 61400-1 standard [7] and cover a wide range of wind conditions, typically determined by offline aero-hydro-servo-elastic simulations. One shortcoming of this testing strategy is that it requires significant modification to the native nacelle controller. The modified controller must bypass monitoring of subsystems that are not physically present on the test bench,

such as blade pitch, yaw, and condition monitoring elements. Therefore, little is learned about the performance of the nacelle controller from this type of testing.

Testing of electrical loads/grid conditions are mainly derived from the IEC 61400-21 standard [8] that specifies the procedures for measurement of electrical characteristics, assessing power quality, and grid compliance of the turbines. Electrical testing typically involves emulating specific grid events such as Low Voltage Ride Through (LVRT), Zero Voltage Ride Through (ZVRT), or other grid faults or conditions that affect the turbine during normal operation. While executing such tests, it may also be of interest to assess the performance of mechanical components within the drivetrain in response to electrical loads/events. For example, an LVRT event induces large torque reversals through the drivetrain and it is important to understand the impact of these loads on specific components. However, when mounted on a test bench, the test article is missing the rotor (hub and blades) and the tower which significantly alters its boundary conditions thereby changing the dynamic characteristics of the drivetrain leading to responses that are different from field testing.

1.2 Hardware-In-the-Loop Implementation

Implementing a test bench with Hardware-in-the-Loop is a more advanced testing strategy compared to testing using predetermined DLCs and is necessary to evaluate the performance of the nacelle controller more effectively [9]. HIL testing enables performance characterizations and electro-mechanical certification testing during a variety of operating conditions with the real nacelle controller. It is advantageous to test the controller in a controlled environment in this way due to the challenge of testing in the field, where conditions are mostly uncontrollable. To implement HIL, a real-time simulation of the full turbine is coupled to the physical nacelle on the test bench. The simulation model in the testing system accounts for the missing components, including the rotor, tower, platform, and actuator models of the blade pitch and yaw system that communicate with the physical nacelle controller.

Researchers have worked extensively in the past to create means for modeling wind turbine dynamics that can ultimately be useful for implementing HIL. The author of [10] created the FAST program, which combines aerodynamic, hydrodynamic, control, electrical system, and structural dynamics models that enables real-time aero-hydro-servo-elastic simulations for a variety of wind turbine configurations, including a baseline 5MW wind turbine developed as an example. The

TurbSim tool created by [11] enables simulation of stochastic turbulent wind fields to be incorporated into FAST. The same researchers have incorporated the tools from TurbSim and FAST into the multibody simulation software, Simpack, and the 5MW baseline Simpack model [12] is used in the case studies of this thesis.

The use of multibody simulation software expands the capabilities of wind turbine dynamics modeling by allowing for much more detailed representations of the wind turbine components, such flexible bodies and detailed gear element modeling. One study performed an in-depth analysis of how the component model fidelity level affected the accuracy of a wind turbine drivetrain under various criteria [13]. A similar study is conducted in Chapter 2 of this thesis.

A few researchers have published work related to HIL implementation for wind turbine nacelle test benches, although it is a relatively new topic. The authors of [14] presented a strategy for creating an HIL system for Clemson University's 7.5MW wind turbine dynamometer test bench and concluded that it was feasible using a simulation model in parallel to the device under test. In a different study, the same authors also characterized the effect of changing boundary conditions for an onshore nacelle in a simulation environment [15]. This thesis builds upon this feasible HIL strategy by addressing considerations that must be made to ensure the nacelle experiences realistic conditions seen in the field.

1.3 Considerations for Hardware-In-the-Loop

For successful implementation of HIL testing, two important considerations must be made. First, the HIL setup must be able to solve the full wind turbine model in real-time to provide the dynamic loads to be applied at the test bench and to provide the physical controller with all of the information it needs to operate. The full wind turbine model used in HIL must be as computationally light as possible so that it may reliably run in real-time, while not sacrificing accuracy of the simulation.

Furthermore, for successful implementation of HIL, it is necessary to characterize the influence of different boundary conditions between the two nacelles in the setup; namely, the nacelle model within the full turbine simulation and the actual nacelle mounted on the test bench without the rotor, tower and platform. While emulating the missing components in the simulation environment allows external loading to be replicated, it may not be possible to accurately reproduce the

forced and free responses on the test bench without physically accounting for the inertia and stiffness of the missing elements or virtually using controller design. As such, it is important to assess the resulting differences due to the abstraction and evaluate any impact it may have on certification tests.

1.4 Aims and Outline of Thesis

This thesis is a simulation based case study where a Simpack multi-body model (developed by [16]) of the National Renewable Energy Laboratory's (NREL) 5 MW baseline wind turbine [12] is used. The aim of this thesis is to address the aforementioned considerations for implementing HIL and develop a strategy for compensating for differences in boundary conditions in nacelle testing.

This thesis contains four chapters. Chapter 2 presents a previous publication by the author that comprises part of the scope of this thesis. In the previous study, the 5MW baseline model with an offshore floating platform is first utilized through a sensitivity analysis to study the influence of varying the fidelity of various components within the drivetrain on the turbine's dynamic responses. The same model is then used to characterize the influence of change in boundary conditions when a nacelle is abstracted from an offshore wind turbine and directly mounted on a test bench without the rotor, tower and platform, with a particular interest in the effect on torsional dynamics. Chapter 3 presents a method that exploits the test bench speed controller to correct the torsional dynamics of the abstracted nacelle. In Chapter 4, the main conclusions from the studies are summarized and the outcomes are discussed.

Chapter 2

Model Fidelity Study and Influence of Boundary Conditions

This chapter is an excerpt from a previous publication [17] that studies the modeling considerations for testing nacelles with hardware-in-the-loop for an offshore floating wind turbine. This work was originally published by ASME for the 2020 IDETC-CIE conference, and ASME has granted permission for the text to be included in this thesis. In this work, a Simpack multi-body model developed by [16] of the National Renewable Energy Laboratory's (NREL) 5 MW baseline model is first utilized through a sensitivity analysis to study the influence of varying the fidelity of various components within the drivetrain on the turbine's dynamic responses. The same model is then used to characterize the influence of change in boundary conditions when a nacelle is abstracted from an offshore wind turbine and directly mounted on a test bench without the rotor, tower, and platform. A similar study previously analyzed the effect of abstraction for testing of onshore wind turbine nacelles [15]. This study extends the analysis to a floating offshore wind turbine with a semi-submersible platform. The results from the aforementioned fidelity and influence of abstraction analyses are utilized to make key recommendations to be considered while developing the HIL setup.

2.1 Model Description

Fig. 2.1 depicts the 5MW offshore wind turbine model adopted for this study. The major subsystems include the rotor, nacelle, tower, and semi-submersible platform.

Figure 2.1: Full offshore wind turbine with semi-submersible floating platform.

As shown in Fig. 2.2, the drivetrain in the nacelle consists of the main shaft, a three stage planetary gearbox, and a high speed coupling which connects the gearbox to the generator. The bedplate supports the drivetrain components through a three-point suspension. In this configuration, the main shaft, which is rigidly connected to the rotor, is supported by a single main bearing, whereas the gearbox is supported through elastomeric mounts at the two torque arms. The bedplate also supports the generator elastically using four mounts at the generator frame. The high speed shaft that couples the gearbox to the generator has high torsional stiffness and some compliance in bending that allows it to transmit rotational motion while being misaligned. Finally, the rotor-nacelle assembly is connected to the tower through the yaw bearing.

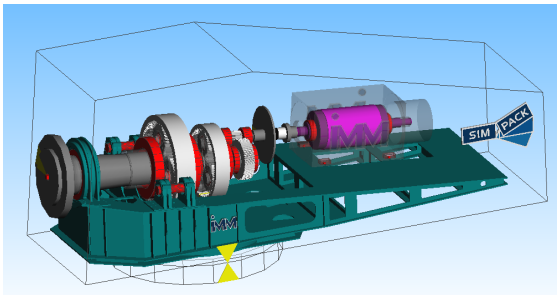

Figure 2.2: Nacelle of the 5MW offshore wind turbine.

2.2 Analysis Approach

In the first part of this study, a sensitivity analysis is conducted to understand the influence of fidelity level of the turbine model on its dynamic behavior. The flexibility or rigidity of the structural elements and the number of degrees-of-freedom (DOF) considered in the mechanical components within the drivetrain are varied systematically to define the different levels of fidelity. Specifically, the main shaft and bedplate are varied from rigid to flexible structural elements for the low and high fidelity levels, respectively. For the flexible configuration, the first three modes are considered for the main shaft and the first six modes are considered for the bedplate. The gearbox supports at the torque arms are switched from rigid connections to elastic mounts, using bushing elements, allowing gearbox motion relative to the bedplate. Within the gearbox, the gears are changed from rigid to flexible gear bodies while the shafts' supports are changed from rigid connections with single DOF revolute joints to elastic bushing elements with 6 DOF bearing representation. Combinations of those variables are formed to obtain six variations of the drivetrain model with increasing fidelity. The resulting response characteristics from these configurations are then analyzed and compared. The main focus of this analysis is on the torsional dynamics that are necessary to perform electro-mechanical certification tests with the HIL setup. Hence, a convergence analysis is carried out to determine the minimum fidelity level that accurately captures the first torsional frequency.

To analyze the influence of abstraction, the responses of a complete offshore wind turbine model (WT) with wind and wave/hydrodynamic inputs are captured. In this model, a semi-submersible floating platform is used which utilizes buoyancy force to hold the turbine at the water surface and for stabilization. Mooring lines are typically used to prevent the wind turbine from drifting/floating away. In the simulation of the complete turbine, the generator torque and blade

pitch are actively controlled to regulate the wind turbine's power. Two hydrodynamic load scenarios with identical fully turbulent wind loads are considered. The first scenario uses still water for hydrodynamic loads, while the second scenario introduces wave loading. The hub loads and generator torque are extracted from the full turbine simulation for both loading scenarios and applied to the abstracted nacelle-only model (DRT). An ideal test bench is assumed wherein the nacelle is subjected to a six-dimensional load vector at the main shaft interface and an ideal air gap torque in the generator. It is worth mentioning that the influence of test bench components and the interface with the nacelle is not considered in this study and will be addressed in a separate study. The results from the full turbine and the abstracted nacelle simulations are then compared.

2.3 Model Fidelity Study

Six nacelle models with increasing fidelity level are considered in this study. The analysis begins with the simplest, lowest fidelity configuration of the nacelle. Table 2.1 summarizes the most basic configuration, which will be called fidelity case (1). The next five cases are configured such that for each case, the complexity of the nacelle components are increased one component at a time until the highest fidelity configuration is reached. Case (2), (3), (4), (5), and (6) increase the fidelity of the main shaft, gearbox supports also known as torque arms, gear bearings, gear bodies, and the bedplate, respectively.

Table 2.1: Base Fidelity (Case 1) Description

Component	Property
Torque arms	Rigid
Main shaft	Rigid
DOF for gear bearings	1 (rotation only)
Gear bodies	Rigid
Bedplate	Rigid
Rotor	Flexible
Tower	Flexible
DOF for platform	6
Torsional mode frequency	4.90 Hz

Each nacelle model is integrated with the rotor, tower, and platform and a free response analysis is performed to capture the first torsional frequency of the complete turbine. The tower and rotor are left flexible and the platform allowed to float with six degrees of freedom so that the results reflect the interaction with realistic boundary conditions. To ensure that all gear pairs are

engaged and avoid model discontinuities, the drivetrain is preloaded from both ends. A constant external torque is applied at the generator, and an opposing torque of equal magnitude times the gearbox ratio is applied to the rotor. The torque value of 42500 Nm is chosen for this simulation as it corresponds to the rated torque of the generator in the 5MW turbine model. A 30 second simulation is then run so that the preloaded turbine reaches static equilibrium. To obtain the torsional frequency of the turbine, a step change in the turbine's torque is applied and the resulting transient torsional response at the main shaft is analyzed as shown in Fig. 2.3.

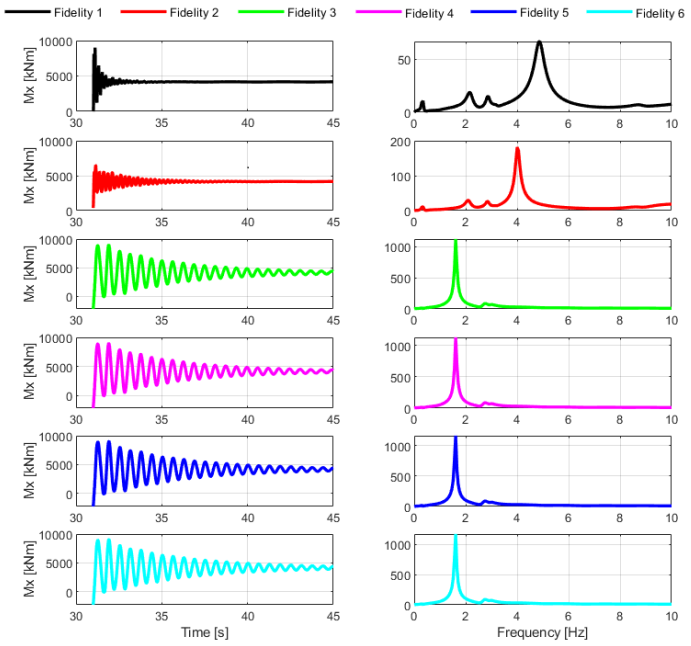

Figure 2.3: Free response test main shaft reaction torque for various nacelle model fidelities and the corresponding spectra.

Table 2.2 summarizes the fidelity cases and their torsional frequencies. The results from this analysis show that the first torsional mode of the drivetrain converges to about 1.6 Hz as fidelity is increased. It is clear that the flexibility of the main shaft and gearbox torque arms has the most significant effect on the first torsional mode of the drivetrain while the other components show little to no influence. As such, modeling the main shaft and gearbox torque arms with the appropriate level of fidelity is sufficient to capture the torsional dynamics of drivetrain accurately. This is an important result because it implies that the rest of the drivetrain components can be simplified significantly thereby reducing the computational load during real-time implementation of the model for HIL testing, particularly to assess electro-mechanical responses.

Table 2.2: Fidelity Variations

Fidelity case	Addition from previous	Torsional mode
1	N/A, most basic components	4.90 Hz
2	Flexible main shaft	4.00 Hz
3	Elastomeric torque arms	1.62 Hz
4	Gear bearings with 6 DOF	1.62 Hz
5	Flexible gear bodies	1.60 Hz
6	Flexible bedplate	1.60 Hz

2.4 Influence of Abstraction

In a floating offshore wind turbine, the nacelle yaw bearing is connected to the tower, which is fixed at its base to the floating platform, and the main shaft is attached to the rotor hub. An abstracted nacelle on a test bench experiences significantly different boundary conditions. The yaw bearing is locked and rigidly attached to the ground, and the main shaft is attached to a load application unit. The goal of this analysis is to examine the extent to which the differences in boundary conditions can influence full-scale nacelle testing in general, and operational testing in a HIL setup.

2.4.1 Free Response Analysis

The turbine model with the highest fidelity nacelle configuration, case (6), is utilized. New cases (6.1), (6.2), and (6.3) are introduced with changes to the boundary conditions seen by the nacelle. Each additional case incrementally brings the nacelle closer to boundary conditions on a test bench. Case (6.1) locks the platform. Case (6.2) locks the platform and makes the tower rigid. Finally, case (6.3) restricts the platform to 0 degrees of freedom and rigid tower and blades. Case (6.4) is also introduced to represent a fully abstracted nacelle on an ideal test bench. A free response analysis similar to the one described in the previous section is performed with focus on torsional characteristics. A summary of the cases and the corresponding frequencies is shown in Table 2.3. The results show that the platform degrees of freedom and tower flexibility do not noticeably affect the torsional mode of the drivetrain. However, making the blades rigid instead of flexible increased the mode frequency from 1.60 to 1.84 Hz. Additionally, removing the blades for the abstracted nacelle case (6.4) increases the frequency further to 1.95 Hz.

Table 2.3: Boundary Conditions Variations

Fidelity	Addition from previous	Torsional mode
6	N/A, real WT conditions	1.60 Hz
6.1	0 DOF Platform	1.60 Hz
6.2	Rigid tower	1.60 Hz
6.3	Rigid blades	1.84 Hz
6.4	Abstracted nacelle	1.95 Hz

2.4.2 Forced Response Analysis

In this analysis, the effect of differences in boundary conditions between the WT and DRT models is studied using the same nacelle model, case (6), with external wind and wave excitations. The combination of wind loads, hydrodynamic loads, and controller responses determine the dynamic response experienced by the components in the drivetrain. Two load cases for the full offshore wind turbine are considered: (1) a fully turbulent, 12 m/s characteristic hub velocity wind field shown in Fig. 2.4 and still water, and (2) an identical wind field with 2 meter trough-to-crest waves with a period of 10 seconds. The wind and wave conditions represent typical conditions seen offshore. Each case was simulated for a 600 second duration. The long time integration ensured that the responses of both cases are compared under steady-state conditions. A comparison of responses are first presented for the still water case, and then differences in simulation results are highlighted when wave excitation is added.

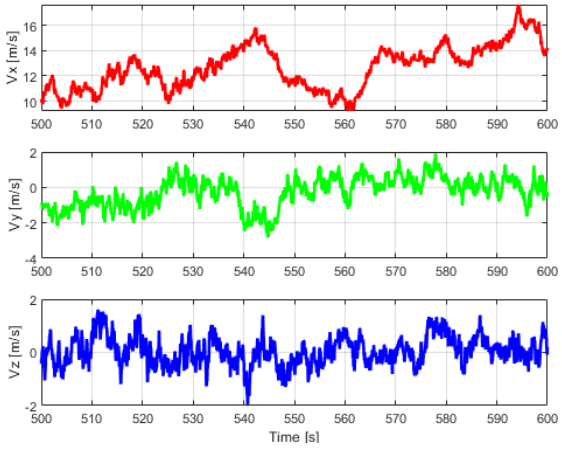

Figure 2.4: Hub center wind velocities.

The resulting hub point reactions from the full turbine (WT) simulation under the first load case, with still water and turbulent wind loads, are depicted in Fig. 2.5. Fig. 2.6 shows the generator

speed, torque, and the power throughout the simulation.

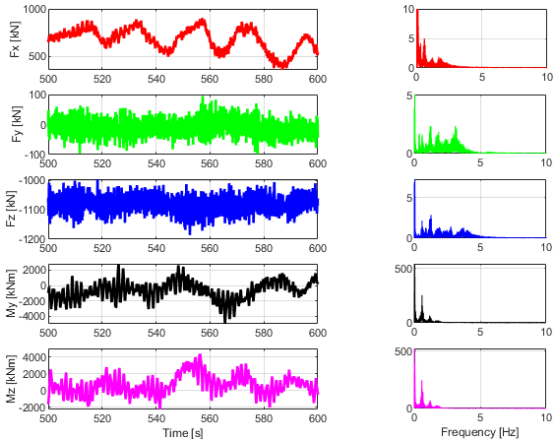

Figure 2.5: Hub loads extracted from full model (WT) simulation with still water.

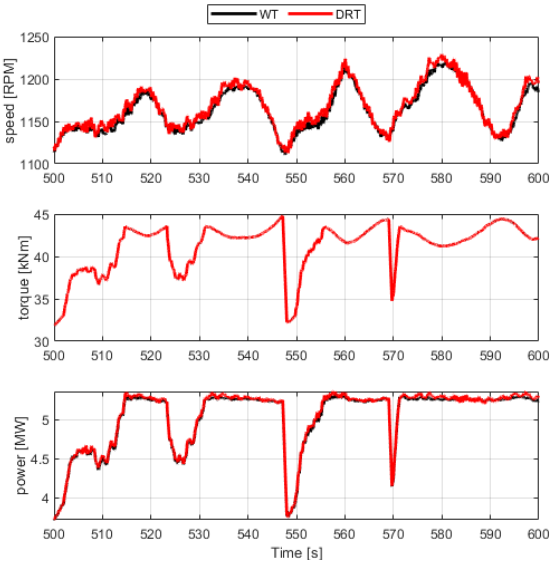

Figure 2.6: Generator operating conditions experienced during full wind turbine (WT) simulation and abstracted nacelle-only (DRT) simulation.

Next, the abstracted nacelle model (DRT) is subjected to the same hub loads and generator torque to capture the response of the drivetrain and compare with that obtained from WT simulation. Fig. 2.6 shows that there are notable differences in the speed and power responses of the generator between the WT and DRT simulations. Specifically, the generator speed in the DRT exhibits relatively amplified oscillations which occur at a frequency of approximately 1.95 Hz as shown in Fig. 2.7. This frequency corresponds to the first torsional mode of the drivetrain as obtained from the

free response analysis. The shift in torsional frequency from 1.60 Hz to 1.95 Hz and the amplification of the torsional oscillations is mainly attributed to the reduction in inertia and damping caused by the absence of the rotor. These oscillations lead to the differences observed in the output power curves.

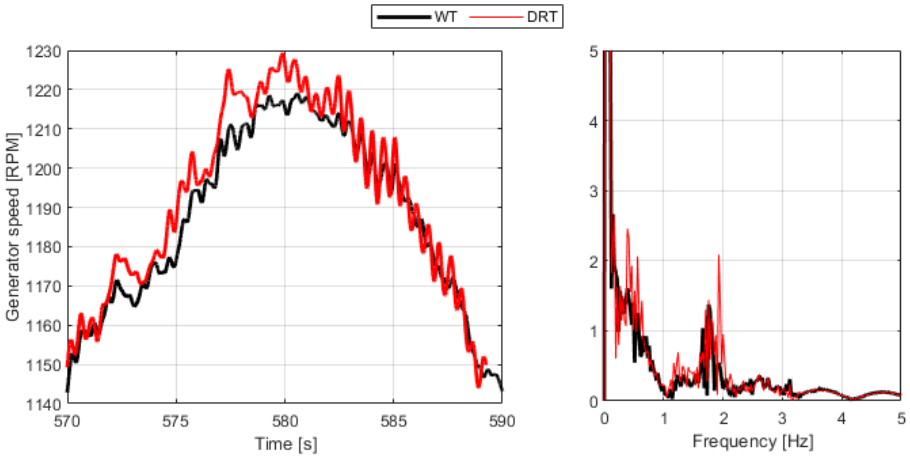

Figure 2.7: Generator speed zoomed in (left) and the corresponding spectra (right) experienced during full (WT) simulation and abstracted nacelle-only (DRT) simulation.

The responses of other components along the drivetrain can also be impacted by these torsional oscillations. One obvious response is the gearbox rolling motion, with respect to the bedplate, as the gearbox supports react to torque. As shown in Fig. 2.8, the right hand side torque arm reaction forces in the vertical, horizontal, and axial directions are compared for the WT and DRT models. The results indicate that the first torsional mode of 1.95 Hz is visible in the frequency response of the vertical torque arm reaction force. For HIL testing, it is necessary to consider re-tuning torsional dampers or implementing inertia compensation techniques to match the torsional dynamic responses of the real nacelle with the nacelle within the the full-turbine real-time simulation environment.

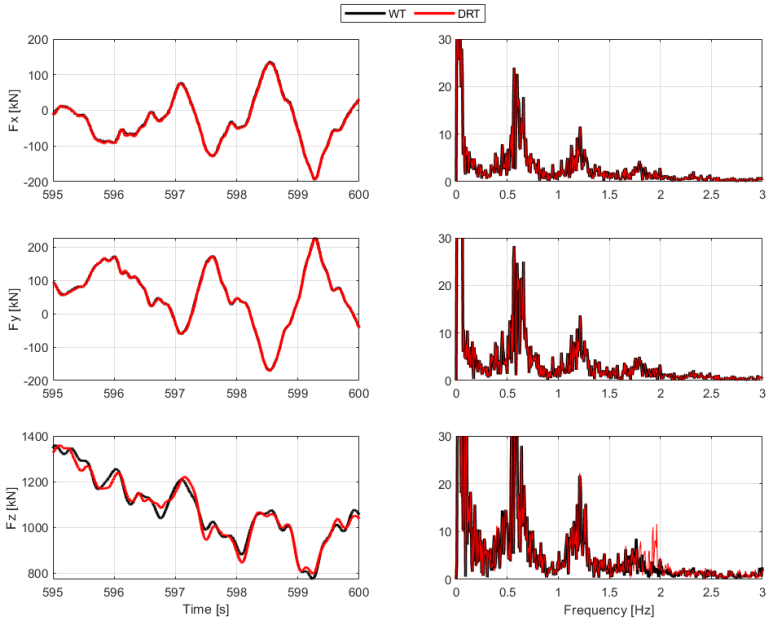

Figure 2.8: Right hand side gearbox torque arm reaction forces (left) and the corresponding spectra (right) experienced during full wind turbine (WT) simulation and abstracted nacelle-only (DRT) simulation.

As shown in Fig. 2.9 and Fig. 2.10, reaction forces and moments at the yaw bearing are also examined. Reactions at the yaw bearing show significant differences between the frequency response of the DRT and WT model. For the WT model, the reactions are at the joint between the yaw bearing and the tower whereas for the DRT, the yaw bearing joint is fixed with 0 degrees of freedom to the reference frame. As shown in Fig. 2.10, similar to the torque arm and generator responses, the rolling reaction torque (Mx) at the yaw bearing shows a torsional frequency shift from 1.6 Hz to 1.95 Hz. However, another significant response difference becomes evident when observing the reaction forces at the yaw bearing in Fig. 2.9. Fig. 2.5 shows an array of force excitation frequencies between 0 and 5 Hz that are inherent to the wind loading. Fig. 2.9 shows reactions to these force excitation frequencies being concentrated at the yaw bearing for the DRT. Unlike the full wind turbine, the abstracted nacelle is fixed rigidly at the yaw bearing. All of the excitation frequencies from the hub loads appear in the yaw reaction forces for the DRT model. The presence of flexibility in the tower acts essentially as a low-pass filter that dissipates these frequencies for the WT model. As such, there is a need to apply appropriate filtering on the loads before they are used as inputs to a test bench.

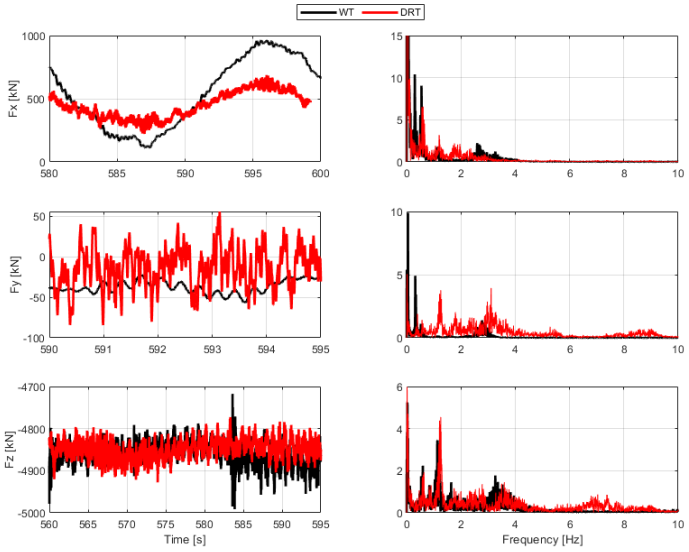

Figure 2.9: Yaw bearing reaction forces (left) and the corresponding spectra (right) experienced during full (WT) simulation and abstracted nacelle-only (DRT) simulation with still water.

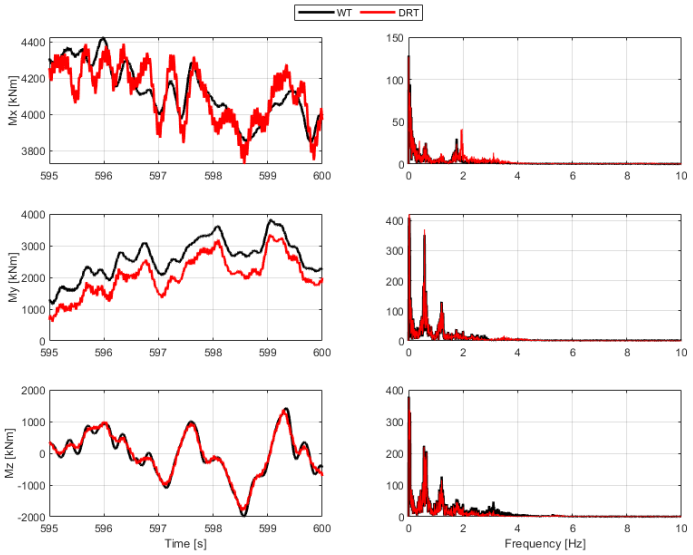

Figure 2.10: Yaw bearing reaction moments (left) and the corresponding spectra (right) experienced during full (WT) simulation and abstracted nacelle-only (DRT) simulation with still water.

Load case (2) adds wave excitation not present in the previously discussed results. The waves have a regular period of 10 seconds with a trough-to-crest height of 2 meters. The excitation frequency of 0.1 Hz due to waves is much lower than any excitation frequency seen in the wind profile. Extracted hub loads shown in Fig. 2.11 show some wave effect on low hub load frequencies

and no difference in high-frequency response, when compared to Fig. 2.9. The thrust load at the hub now shows an excitation that matches the frequency of the waves. Fig. 2.12 shows that the frequency of the waves also carries over to the yaw bearing reaction in the x-direction. However, adding wave excitation to the simulation shows no noticeable differences in the high frequency responses of the drivetrain components, when compared to the still water case. It is worth reiterating that this study is mainly focused on analyzing the torsional dynamics in the drivetrain and therefore, some additional differences observed in the frequency spectra, particularly in the low frequency range for the yaw bearing thrust and lateral reaction forces from Fig. 2.9 and Fig. 2.12, are not addressed here and will be investigated in the future.

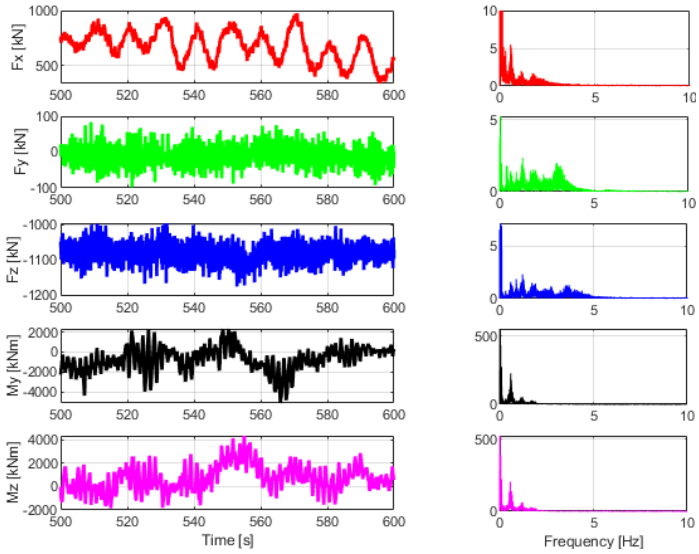

Figure 2.11: Hub loads extracted from full model (WT) simulation with 2 meter regular waves.

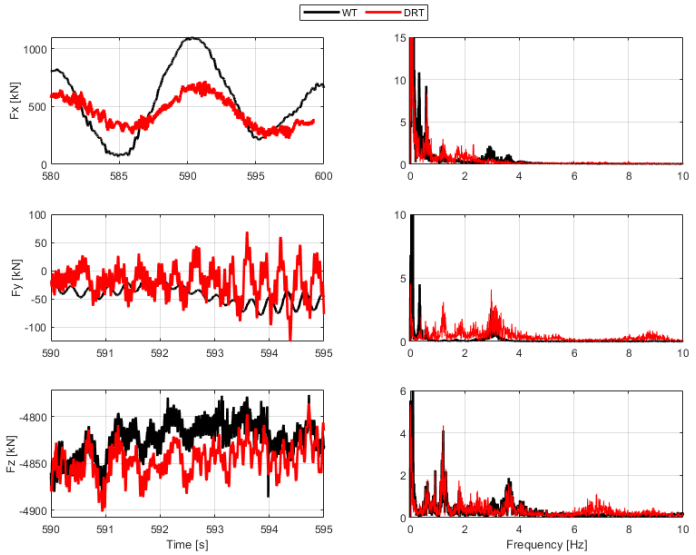

Figure 2.12: Yaw bearing reaction forces (left) and the corresponding spectra (right) experienced during full (WT) simulation and abstracted nacelle-only (DRT) simulation with waves.

Chapter 3

Torsional Compensation Methods

This chapter is an excerpt from a previous article [18] published as part of the proceedings of the 2021 Conference for Wind Power Drives hosted by RWTH Aachen University. The original publishers have granted permission to use the article as part of this thesis.

A simulation case study was utilized in Chapter 2 to demonstrate the differences in torsional characteristics between field testing and full-scale nacelle testing with an ideal test bench. It was shown that the frequency of the first torsional mode of the drivetrain increases in the absence of the rotor. For accurate execution of electro-mechanical certification tests, it is important that the torsional dynamic behavior of the nacelle on the test bench closely resembles that of a nacelle in the field. Several efforts have been made to address these differences and develop control techniques to emulate the missing inertia and replicate eigenfrequencies such that field testing can be better reproduced on a test bench, including a similar study conducted in [19].

This work extends such studies to the 7.5 MW test bench at the Clemson WTDTF by considering the differences in the test bench setup and operating mode. Specifically, the asynchronous drive motor on this test bench operates in speed control mode and is coupled to the LAU through a high-speed coupling and a reduction gearbox. In this chapter, pole placement control techniques are utilized to compensate for those variations and shift the torsional frequency of the test bench-nacelle assembly to match that of the full turbine. This will enable the development of a Hardware-In-the-Loop testing platform to allow for full turbine operational testing with native nacelle controller and perform more realistic electromechanical certification tests. This chapter is organized as follows: Section 3.1 introduces lumped-parameter models used to understand the baseline torsional char-

acteristics of the nacelle coupled to the test bench versus that coupled to the rotor. Section 3.2 discusses pole placement technique to match the torsional characteristics using two forms of the test bench speed controller, PI and PID. Section 3.3 extends the analysis for higher fidelity models of the nacelle and test bench. In Section 3.4, the performance of the tuned controller is evaluated under two test scenarios: Low Voltage Ride Through (LVRT), and a highly dynamic turbulent wind input.

3.1 Lumped-Parameter Modeling and Analysis

A simplified 3-DOF lumped parameter torsional model is introduced to represent the coupled nacelle-test bench system. The nacelle part is represented by a 2-DOF system with symmetric inertia ($J_{Mid} = J_{Rear}$), stiffness ($k_1 = k_2$), and damping values ($d_1 = d_2$) while the test bench is represented by the LAU disk inertia, (J_{LAU}). The stiffness and damping values are chosen such that the first and second torsional modes of the 3-DOF system nearly match the corresponding modes obtained from a higher fidelity Simpack model of the same system. A diagram of the simple model is shown in Fig. 3.1 with the controller input torque (T_{in}) applied to the LAU body. The generator torque from the nacelle controller is not considered for simplicity.

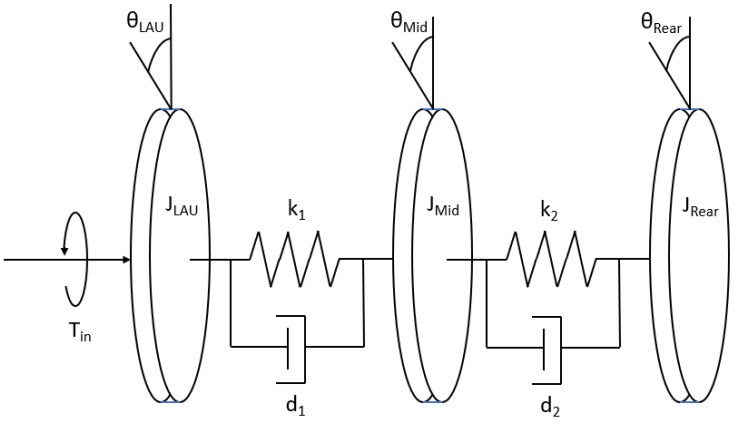

Figure 3.1: Representation of coupled nacelle-test bench as a torsional 3 mass-damper-spring system

The equations of motion for the 3-DOF system can be written as shown in equations (3.1), (3.2), (3.3), where, θ_{LAU} represents the angular displacement of the LAU disk, θ_{Mid} represents the angular displacement of the first drivetrain mass, and θ_{Rear} represents the angular displacement of

the second drivetrain mass. The dot represents derivative with respect to time.

$$J_{LAU}\ddot{\theta}_{LAU} + k_1(\theta_{LAU} - \theta_{Mid}) + d_1(\dot{\theta}_{LAU} - \dot{\theta}_{Mid}) = T_{in} \tag{3.1}$$

$$J_{Mid}\ddot{\theta}_{Mid} + k_1(\theta_{LAU} - \theta_{Mid}) + d_1(\dot{\theta}_{LAU} - \dot{\theta}_{Mid}) + k_2(\theta_{Mid} - \theta_{Rear}) + d_2(\dot{\theta}_{Mid} - \dot{\theta}_{Rear}) = 0 \tag{3.2}$$

$$J_{Rear}\ddot{\theta}_{Rear} + k_2(\theta_{Mid} - \theta_{Rear}) + d_2(\dot{\theta}_{Mid} - \dot{\theta}_{Rear}) = 0 \tag{3.3}$$

An eigenvalue analysis is performed using the simplified lumped-parameter model to obtain the first two torsional eigenfrequencies which were found to be 5.80 Hz and 16.3 Hz. The equivalent system is created in Simpack, except the LAU body and controller are removed and the two-body drivetrain connects to the flexible rotor instead, as shown in Fig. 3.2, where the blades are modeled with 53 nodes each. The eigenvalue analysis was repeated in Simpack to obtain the first two torsional modes of the nacelle-rotor model as 1.88 Hz and 3.22 Hz, which are the desired pole locations for pole placement.

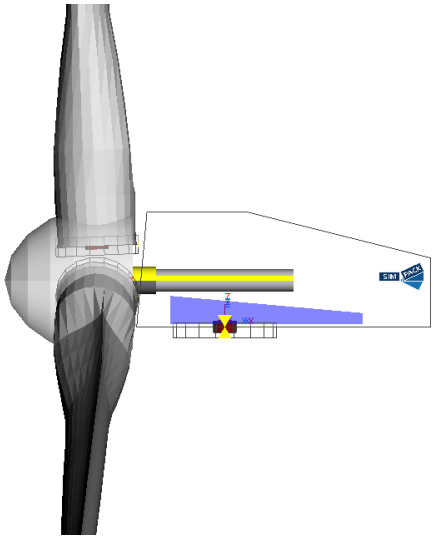

Figure 3.2: Simpack model of two-body nacelle drivetrain coupled with flexible rotor

3.2 Pole Placement for 3-DOF System

3.2.1 Pole Placement Using a Proportional-Integral Controller

The input torque from the test bench speed controller is represented by equation (3.4).

$$T_{in} = K_P(\dot{\theta}_{LAU,set} - \dot{\theta}_{LAU}) + K_I \int \dot{\theta}_{LAU,set} - \dot{\theta}_{LAU}\, dt \tag{3.4}$$

Here K_P is the proportional gain acting on the error between the set ($\dot{\theta}_{LAU,set}$) and actual LAU speeds ($\dot{\theta}_{LAU}$), and K_I is the integral gain acting on the integral of the feedback error. For the sake of simplicity, the reference speed ($\dot{\theta}_{LAU,set}$) is zero for this analysis. Using the torque equation 3.4, and the equations of motion for the three-body system (3.1), (3.2), (3.3), the closed-loop model with a PI controller can be represented in state space form as shown in equation (3.5).

$$\begin{pmatrix} \dot{x}_1 \\ \dot{x}_2 \\ \dot{x}_3 \\ \dot{x}_4 \\ \dot{x}_5 \\ \dot{x}_6 \\ \dot{x}_7 \end{pmatrix} = \begin{pmatrix} 0 & 0 & 0 & 0 & 1 & 0 & 0 \\ 0 & 0 & 0 & 0 & 0 & 1 & 0 \\ 0 & 0 & 0 & 0 & 0 & 0 & 1 \\ 0 & 0 & 0 & 0 & -\frac{K_I}{K_P} & 0 & 0 \\ -\frac{k_1}{J_{LAU}} & \frac{k_1}{J_{LAU}} & 0 & \frac{K_P}{J_{LAU}} & -\frac{K_P+d_1}{J_{LAU}} & \frac{d_1}{J_{LAU}} & 0 \\ \frac{k_1}{J_{Mid}} & -\frac{k_1+k_2}{J_{Mid}} & \frac{k_2}{J_{Mid}} & 0 & \frac{d_1}{J_{Mid}} & -\frac{d_1+d_2}{J_{Mid}} & \frac{d_2}{J_{Mid}} \\ 0 & \frac{k_2}{J_{Rear}} & -\frac{k_2}{J_{Rear}} & 0 & 0 & \frac{d_2}{J_{Rear}} & -\frac{d_2}{J_{Rear}} \end{pmatrix} \begin{pmatrix} x_1 \\ x_2 \\ x_3 \\ x_4 \\ x_5 \\ x_6 \\ x_7 \end{pmatrix} \tag{3.5}$$

State variables 1-3 are the angular positions of the LAU (x_1) and two drivetrain bodies (x_2 and x_3). State variables 5-6 are angular velocity of the LAU (x_5) and two drivetrain bodies (x_6 and x_7). An additional state, (x_4), is defined to represent the integral portion of the PI controller as shown in equation (3.6).

$$x_4 = \frac{K_I}{K_P} \int \dot{\theta}_{LAU,set} - \dot{\theta}_{LAU}\, dt \tag{3.6}$$

By varying the controller gains, K_P and K_I, the effective damping and stiffness characteristics of the closed-loop system can be changed to obtain the desired poles. The root loci of the closed loop A matrix were generated for a range of values of K_P and K_I iteratively. One root locus plot

with a trajectory that passes through desired pole location for the first torsional mode is shown in Fig. 3.3. In this case, the required gains are $1.714 * 10^7$ and $1.463 * 10^9$ for K_P and K_I, respectively.

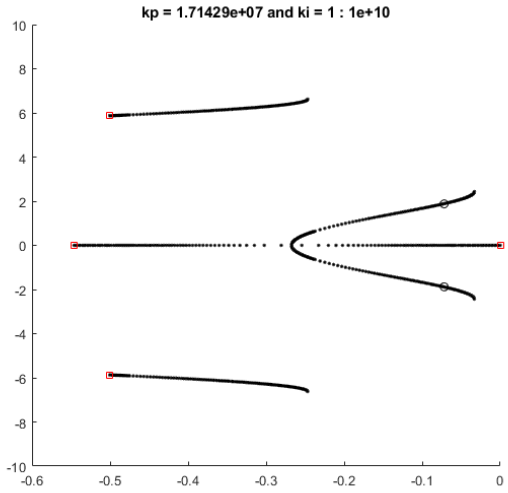

Figure 3.3: Root locus plot for PI closed-loop three-body system with fixed $K_P = 1.714 * 10^7$ and swept K_I

As verification, the step response of the test bench system with the tuned controller is compared with the corresponding response from the full turbine model as shown in Fig. 3.4. The time domain responses of the rotor/LAU velocity are in good agreement with some differences that can be attributed to higher modes that were not matched by the PI controller. This can be seen from the FFT plot where only the frequency of the first torsional mode is emulated successfully.

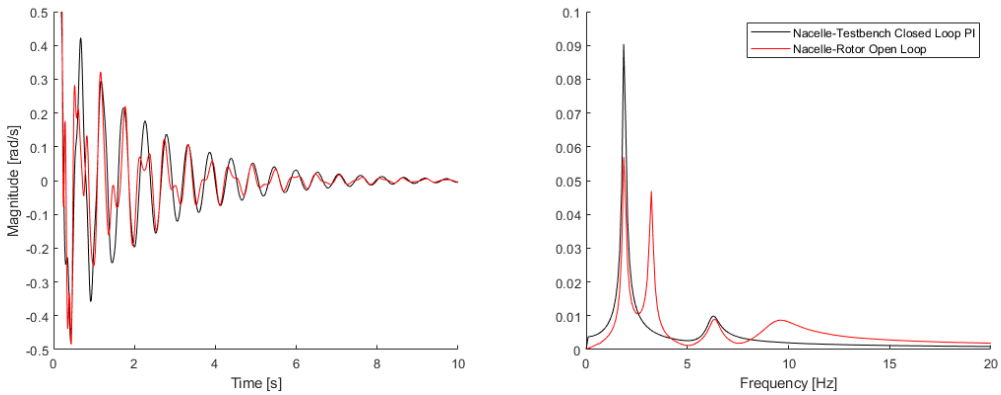

Figure 3.4: Time and frequency domain free response comparison of tuned PI closed-loop three-body system vs. model with rotor

3.2.2 Pole Placement Using a Proportional-Integral-Derivative Controller

The results from pole placement using the PI controller indicate that a PID controller may need to be implemented to better capture the second torsional mode. Compared to proportional an integral controller gains, which represent virtual damping and stiffness respectively, adding a derivative gain can also represent virtual inertia. The equation for the torque from a PID controller is shown in equation (3.7),

$$T_{in} = K_P(\dot{\theta}_{LAU,set} - \dot{\theta}_{LAU}) + K_I \int \dot{\theta}_{LAU,set} - \dot{\theta}_{LAU}\, dt + K_D \frac{d}{dt}(\dot{\theta}_{LAU,set} - \dot{\theta}_{LAU}) \tag{3.7}$$

The controller torque is similar to that from the PI (3.4) but with the derivative gain, K_D acting on the derivative of the error between the set and actual speeds. The closed loop state space representation of the system is given by (3.8).

$$\begin{pmatrix} \dot{x}_1 \\ \dot{x}_2 \\ \dot{x}_3 \\ \dot{x}_4 \\ \dot{x}_5 \\ \dot{x}_6 \\ \dot{x}_7 \\ \dot{x}_8 \end{pmatrix} = \begin{pmatrix} 0 & 0 & 0 & 0 & 0 & 1 & 0 & 0 \\ 0 & 0 & 0 & 0 & 0 & 0 & 1 & 0 \\ 0 & 0 & 0 & 0 & 0 & 0 & 0 & 1 \\ 0 & 0 & 0 & \frac{-1}{T_1} & 1 & \frac{K_D}{K_P T_1^2} - \frac{1}{T_1} & 0 & 0 \\ 0 & 0 & 0 & 0 & 0 & \frac{-K_I}{K_P T_1} & 0 & 0 \\ -\frac{k_1}{J_{LAU}} & \frac{k_1}{J_{LAU}} & 0 & \frac{K_P}{J_{LAU}} & 0 & \frac{-K_D}{J_{LAU} T_1} - \frac{d_1}{J_{LAU}} & \frac{d_1}{J_{LAU}} & 0 \\ \frac{k_1}{J_M} & -\frac{k_1+k_2}{J_M} & \frac{k_2}{J_M} & 0 & 0 & \frac{d_1}{J_M} & -\frac{d_1+d_2}{J_M} & \frac{d_2}{J_M} \\ 0 & \frac{k_2}{J_R} & -\frac{k_2}{J_R} & 0 & 0 & 0 & \frac{d_2}{J_R} & -\frac{d_2}{J_R} \end{pmatrix} \begin{pmatrix} x_1 \\ x_2 \\ x_3 \\ x_4 \\ x_5 \\ x_6 \\ x_7 \\ x_8 \end{pmatrix} \tag{3.8}$$

The state variables 1-3 are the angular position of the LAU body (x_1) and the two drivetrain bodies (x_2 and x_3) while state variables x_6 through x_8 represent their angular velocities. Two additional states are introduced to represent the PID controller as shown in (3.9).

$$\begin{pmatrix} \dot{x}_4 \\ \dot{x}_5 \end{pmatrix} = \begin{pmatrix} \frac{-1}{T_1} & 1 \\ 0 & 0 \end{pmatrix} \begin{pmatrix} x_4 \\ x_5 \end{pmatrix} + \begin{pmatrix} \frac{1}{T_1} - \frac{K_D}{K_P T_1^2} \\ \frac{K_I}{K_P T_1} \end{pmatrix} (\dot{\theta}_{LAU,set} - x_6) \tag{3.9}$$

A time delay (T1) is also included for practical implementation of a PID controller. An

iterative approach similar to the one in Section 3.2.1 is used to generate several root loci corresponding to the 3-dimensional parameter space represented by the different ranges of K_P, K_I, and K_D. A down-selection is performed to keep the root locus that is closest to the desired poles and obtain the corresponding range of gains. The chosen range is then refined, and new root loci plots are generated. This process is repeated until the root locus passing through the desired poles is obtained as shown in Fig. 3.5.

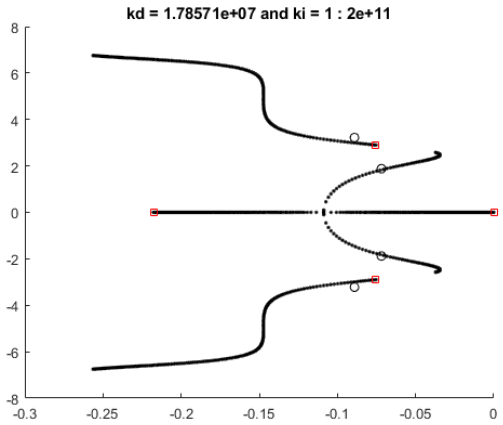

Figure 3.5: Root locus plot for PID closed-loop three-body system with fixed K_P=$3.150 * 10^7$, fixed K_D=$1.786 * 10^7$ and swept K_I

Table 3.1 shows the controller gains resulting from the pole placement method and the eigenfrequencies corresponding to the first two torsional modes. It should be noted that an optimization technique can be utilized to find the controller gains in a more efficient way.

Table 3.1: Tuned controller gains for the PID 3-body system and resulting eigenfrequencies of first and second torsional mode

Model	K_P	K_I	K_D	1st Mode [Hz]	2nd Mode [Hz]
Nacelle with Rotor	-	-	-	1.878	3.221
Nacelle with LAU	$3.150 * 10^7$	$4.008 * 10^9$	$1.786 * 10^7$	1.887	3.217

As discussed in Section 3.2.1, the step response of the full turbine model is compared with that from the test bench nacelle system with the tuned PID controller to verify its accuracy. As shown in Fig. 3.6, the time domain responses of the rotor/LAU velocities are in excellent agreement. The frequency domain results confirm that the emulates of the first two torsional modes on the test bench, which is a remarkable improvement as compared to the PI controller (Fig. 3.4). Some minor deviations are observed at frequencies corresponding to higher modes but their contribution to the

overall response is negligible.

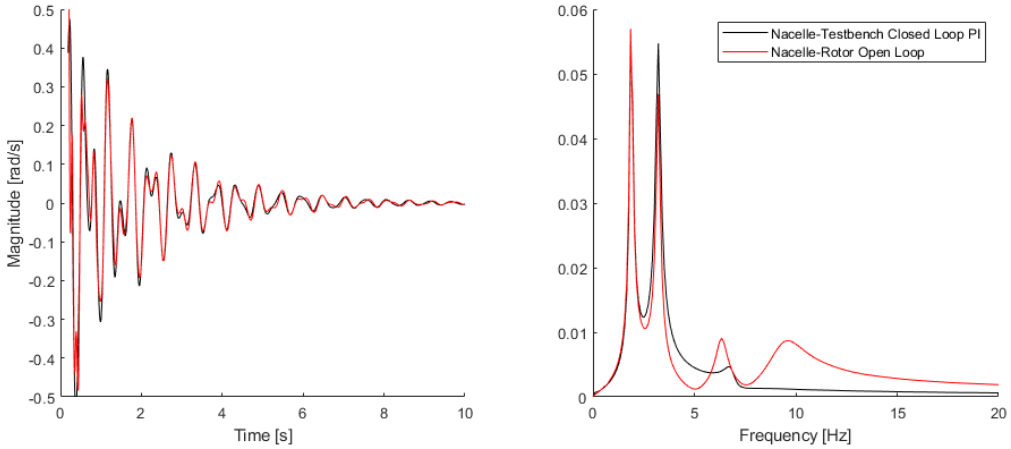

Figure 3.6: Time and frequency domain free response comparison of tuned PID closed-loop three-body system vs. model with rotor

3.3 Pole Placement for Nacelle with Test Bench Model

Results from the case study using the simple 3-DOF model suggest that it is feasible to use the test bench speed controller to emulate the torsional dynamics of a nacelle in the field. In this section, the feasibility of using the pole placement method for a more complex system is investigated. To that end, a detailed Simpack model of a 5MW nacelle coupled to the 7.5 MW test bench components is introduced and the method used to obtain the desired pole locations is described. Next, the state space structure for the nacelle-test bench model with a PI/PID controller is formulated and the pole placement method is discussed.

3.3.1 Description of the Detailed Nacelle and Test Bench Model

As shown in Fig. 3.7, the model used in this case study is a Simpack representation of the detailed 5MW baseline wind turbine nacelle coupled to the 7.5 MW test bench at Clemson University. The components within the nacelle are configured based on the previous model fidelity sensitivity study in Chapter 2. The main shaft and the gearbox supports are modeled as flexible components as they are shown to be important for capturing the torsional dynamic behavior accurately. The high-speed shaft is modeled such that it allows bending deformations and misalignment between the gearbox and the generator. The gearbox model is simplified by using rotational joint representation

for the bearings and assuming zero backlash between gears. The generator stator is rigidly attached to the generator frame and the generator rotor has a single rotational degree of freedom. Finally, the bedplate, gearbox housing, and planet carriers are set as rigid components.

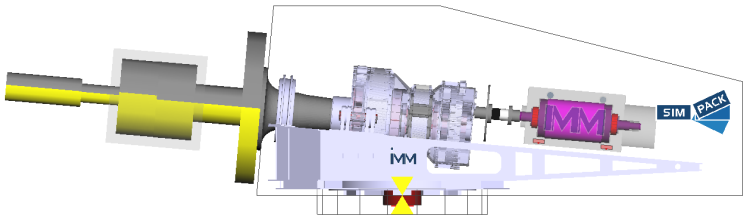

Figure 3.7: Detailed nacelle Simpack model coupled to torsional test bench model

Fig. 3.7 also shows the components included in the test bench model - the motor rotor (rigid), high speed shaft (flexible, also with flexible couplings on either side), 100:1 speed reduction gearbox, low speed shaft (flexible), and the load application disk (rigid). The mass, inertia, stiffness and damping properties for these components are based on actual design values and have been experimentally validated. The test bench model also accounts for the speed controller in which the torque is applied at the motor while the speed is measured at the load application unit disk.

The approach used to obtain the desired values of the poles for this case is similar to the one discussed in Section 3.2. A high-fidelity rotor model with 53 node finite element blades is coupled to the detailed nacelle model at the main shaft, and an eigenvalue analysis is performed in Simpack to obtain the first and second open-loop torsional eigenfrequencies. The real and imaginary components of these two desired pole locations are shown in Table 3.2.

Table 3.2: Open-loop real and imaginary components for detailed nacelle model with rotor

Eigenvalue	Real Component [Hz]	Imaginary Component [Hz]
First	-0.0382	1.644
Second	-0.1164	2.772

3.3.2 Pole Placement Using a Proportional-Integral Controller

The closed loop model of the detailed nacelle-test bench system used in this case study has a total of 45/46 state variables with a PI/PID controller, compared to 7/8 for the simple 3-DOF model, making it difficult to develop a symbolic representation of the system. However, for pole placement, it is only necessary to identify the states that are affected by the controller gains. Equation (3.10)

shows a condensed state space representation of the closed loop detailed nacelle-test bench system with a PI speed controller. The relevant portion of the 45x45 A matrix shows the entries/states that are affected by the controller. The test bench motor inertia is denoted as J_M. The parameters that are not of interest are denoted by the letter "C".

$$\frac{d}{dt}\begin{pmatrix} \vdots \\ x_{23} \\ x_{24} \\ x_{25} \\ x_{26} \\ \vdots \end{pmatrix} = \begin{pmatrix} \ddots & \vdots & \vdots & \vdots & \vdots & \ddots \\ \dots & 0 & \frac{-K_I}{K_P} & 0 & 0 & \dots \\ \dots & 0 & C & 0 & 0 & \dots \\ \dots & 0 & 0 & C & 0 & \dots \\ \dots & \frac{K_P}{J_M} & \frac{-K_P}{J_M} & C & C & \dots \\ \ddots & \vdots & \vdots & \vdots & \vdots & \ddots \end{pmatrix} \begin{pmatrix} \vdots \\ x_{23} \\ x_{24} \\ x_{25} \\ x_{26} \\ \vdots \end{pmatrix} \tag{3.10}$$

In this case, x_{23} is the additional state variable defined to denote the integral portion of the PI controller, x_{24} is the speed of the LAU disk, and x_{26} is the speed of the test bench motor. x_{25} is another state variable that is not relevant to the controller.

Again, the closed loop A matrix is utilized to iteratively generate root loci for a range of values of K_P and K_I. One root locus plot with a trajectory that passes through the pole location corresponding to the first torsional mode is shown in Fig. 3.8.

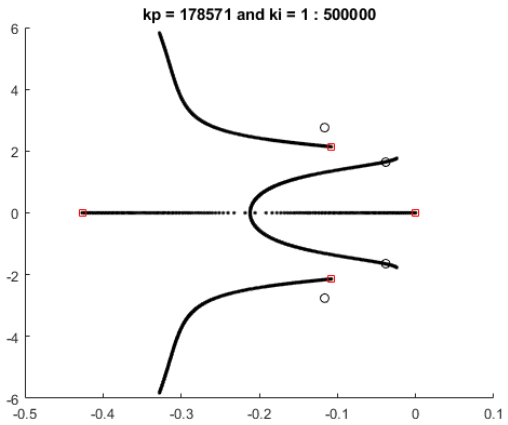

Figure 3.8: Root locus plot for PI detailed coupled nacelle-test bench model with fixed $K_P = 1.786 * 10^5$ and swept K_I

While the pole pair corresponding to the second mode is not considered when selecting gains, it is preferred that damping of the second pole pair is high enough to minimize its effects. The proportional and integral gains that achieve the desired pole placement of the first mode are in

Table 3.3.

Table 3.3: Tuned controller gains for the PI detailed nacelle-test bench model and resulting eigenfrequencies of first and second torsional mode

Model	K_P	K_I	First Mode [Hz]	Second Mode [Hz]
Nacelle with Rotor	-	-	1.644	2.772
Nacelle with LAU	$1.786 * 10^5$	$1.616 * 10^7$	1.641	3.284

3.3.3 Pole Placement Using a Proportional-Integral-Derivative Controller

The pole placement method with a PID controller is the same as that described in the previous section. The truncated state space representation of the closed loop system with a PID controller is shown in (3.11). In this case, due to an additional controller dynamic state, the closed loop A matrix is of size 46x46. As shown in (3.11), five entries in the state matrix are functions of the controller parameters. x_{23} and x_{24} are controller dynamic state variables, x_{25} is the speed of the LAU disk, x_{26} is another state variable not relevant to the controller, and x_{27} is the test bench motor speed.

$$\frac{d}{dt}\begin{pmatrix} \vdots \\ x_{23} \\ x_{24} \\ x_{25} \\ x_{26} \\ x_{27} \\ \vdots \end{pmatrix} = \begin{pmatrix} \ddots & \vdots & \vdots & \vdots & \vdots & \vdots & \ddots \\ \dots & \frac{-1}{T_1} & 1 & \frac{K_D}{K_P T_1^2} - \frac{1}{T_1} & 0 & 0 & \dots \\ \dots & 0 & 0 & \frac{-K_I}{K_P T_1} & 0 & 0 & \dots \\ \dots & 0 & 0 & C & 0 & 0 & \dots \\ \dots & 0 & 0 & 0 & C & 0 & \dots \\ \dots & \frac{K_P}{J_{Motor}} & 0 & \frac{-K_D}{J_{Motor} T_1} - \frac{d_1}{J_{Motor}} & C & C & \dots \\ \ddots & \vdots & \vdots & \vdots & \vdots & \vdots & \ddots \end{pmatrix} \begin{pmatrix} \vdots \\ x_{23} \\ x_{24} \\ x_{25} \\ x_{26} \\ x_{27} \\ \vdots \end{pmatrix} \tag{3.11}$$

The time delay (T1) in (3.11) is chosen to be 0.1 milliseconds, so that the controller is near ideal. Again, the iterative root locus analysis described in Section 3.2.2 is used to determine the root locus that passes through the desired pole locations. The root locus that was found to match the frequency and damping of the first torsional mode and frequency only for the second mode (y coordinate but not x coordinate) of the test bench-nacelle simultaneously is shown in Fig. 3.9.

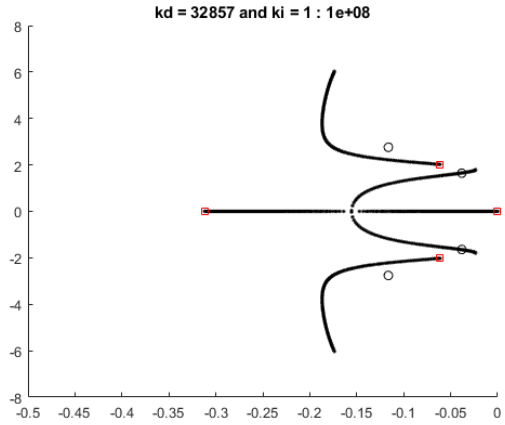

Figure 3.9: Root locus plot for PID detailed coupled nacelle-test bench model with fixed $K_P = 1.850 * 10^5$, fixed $K_D = 3.286 * 10^4$ and swept K_I

Table 3.4 shows the combination of gains that matches the test bench-nacelle system's first two torsional modes with those of the high-fidelity open loop rotor-nacelle system.

Table 3.4: Tuned controller gains for the PID detailed nacelle-test bench model and resulting eigenfrequencies of first and second torsional mode

Model	K_P	K_I	K_D	First Mode [Hz]	Second Mode [Hz]
Nacelle with Rotor	-	-	-	1.644	2.772
Nacelle with LAU	$1.850 * 10^5$	$2.020 * 10^7$	$3.286 * 10^4$	1.647	2.786

3.4 Evaluation of Controller Performance

This section describes the assessment of controller performance under two test scenarios. First, a low-voltage ride through simulation case is used to evaluate the ability of the closed-loop model with both PI and PID controllers to emulate the torsional behavior of the open-loop model. Next, a forced response study is used to evaluate the tracking performance of the test bench with tuned angular speed controller with a highly dynamic reference angular speed profile.

3.4.1 Performance During Low Voltage Ride Through

A requirement of modern wind turbines is that they stay connected to the grid during temporary voltage dips or faults to avoid shutdowns, called a low voltage ride through (LVRT). In a low voltage event, a fault occurs in the electric grid that may cause the generator to release torque

for a short time duration. The testing procedure for an LVRT is described in IEC 61400-21 where a grid simulator is used to create a voltage flicker [8]. For this study, a benchmark LVRT simulation is set up by considering the nacelle coupled with a rotor and subjected to a laminar 8 m/s wind input. As shown in Fig. 3.10, at steady state, the generator torque is dropped to zero for half a second and recovered to represent a grid fault.

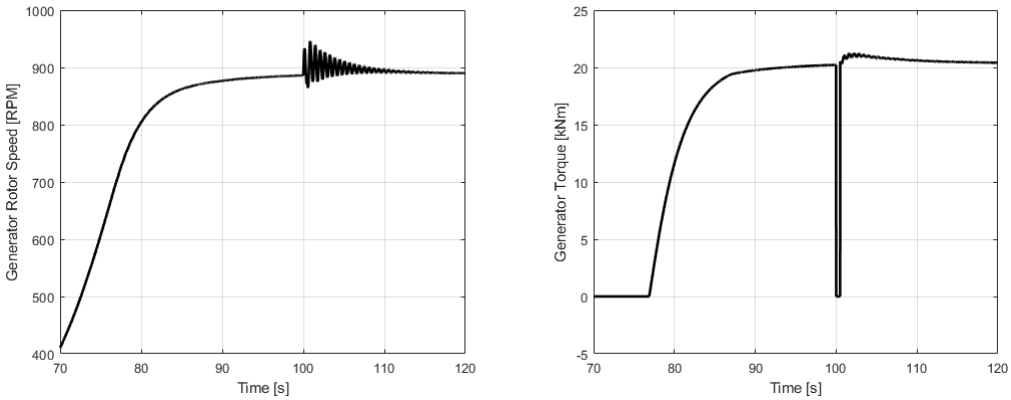

Figure 3.10: Generator speed and torque for LVRT Simulation Case

A similar scenario is simulated using the detailed nacelle model with the tuned PI test bench speed controller. Here, the generator torque is dropped to zero for half a second and recovered while the test bench controller is tracking a near constant speed profile at the LAU. Fig. 3.11 shows a comparison of the generator speeds from the two simulations. It can be seen that there is excellent agreement between the transient responses during the LVRT event as confirmed by the FFT plot. To put things in perspective, the same LVRT event was simulated using a controller with lower PI gains, and as shown in Fig. 3.12, there is a significant mismatch in the responses. These results demonstrate the effectiveness of pole-placement in emulating field responses on a test bench. It should be noted that, as opposed to the simplified turbine model used in Section 3.1, the contribution of the second torsional mode of the detailed turbine model to the overall response is negligible, and therefore, a PI controller may be adequate to emulate the response by matching only the first torsional mode.

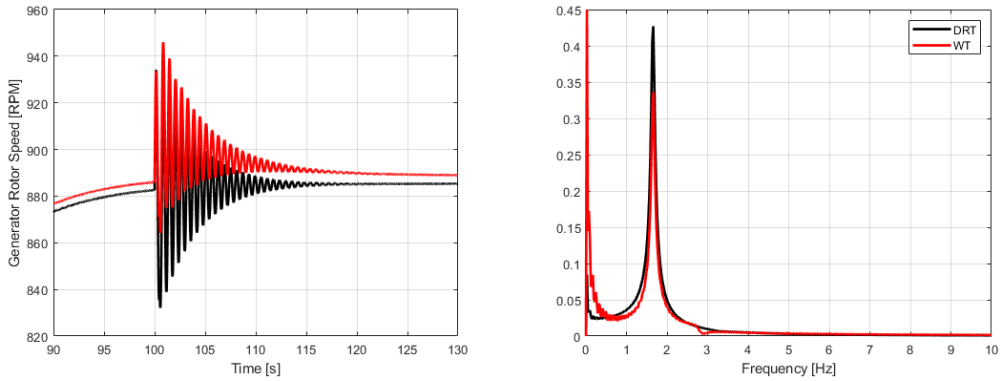

Figure 3.11: LVRT response for coupled detailed nacelle-test bench with tuned PI controller (DRT) model vs. nacelle coupled to flexible rotor (WT).

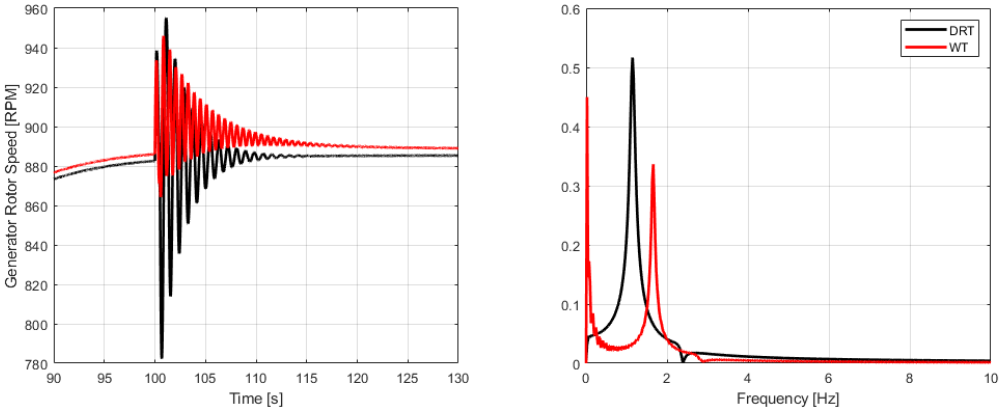

Figure 3.12: LVRT response for coupled detailed nacelle-test bench with low PI controller gains (DRT) model vs. nacelle coupled to flexible rotor (WT).

Next, the detailed nacelle model with the tuned PID speed controller is simulated with the same grid fault event. The results presented in Fig. 3.13 show no improvement compared to the case with the PI controller, because, as mentioned previously, the response is dominated by the first mode.

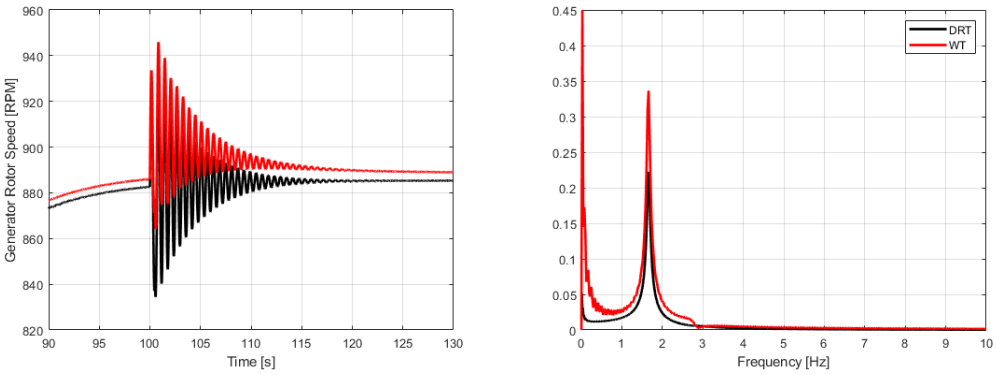

Figure 3.13: LVRT response for coupled detailed nacelle-test bench with tuned PID controller (DRT) model vs. nacelle coupled to flexible rotor (WT).

3.4.2 Forced Response Tracking Performance

The ability of the tuned controllers to track a highly dynamic reference speed profile is evaluated. The reference profile is extracted from an offline simulation of the detailed turbine model subjected to a turbulent wind field with an average speed of 18 m/s, as shown in Fig. 3.14.

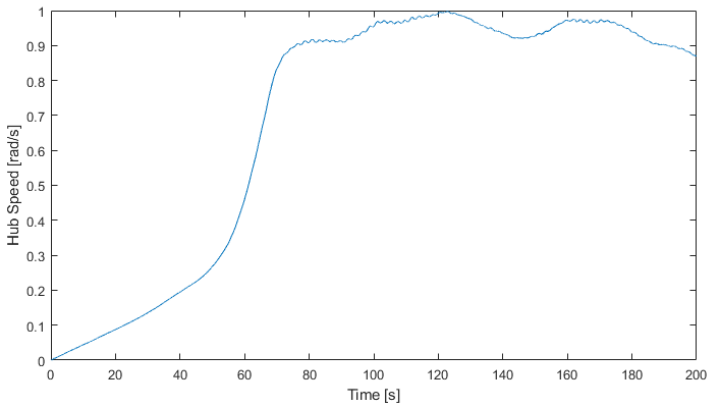

Figure 3.14: Hub speed profile from coupled nacelle-rotor model simulation with 18 m/s turbulent wind

The resulting generator speeds from the turbine and test bench model with a tuned PI controller are shown in Fig. 3.15. Overall the PI controller shows good tracking performance with a Root-Mean-Square (RMS) tracking error of 7.65 RPM over the considered range. This error is mainly due to the amplification of the responses at the first torsional mode resulting from high controller gains. Similar results are observed when using the PID controller as shown in Fig. 3.16. In this case, RMS tracking error is found to be 7.57 RPM.

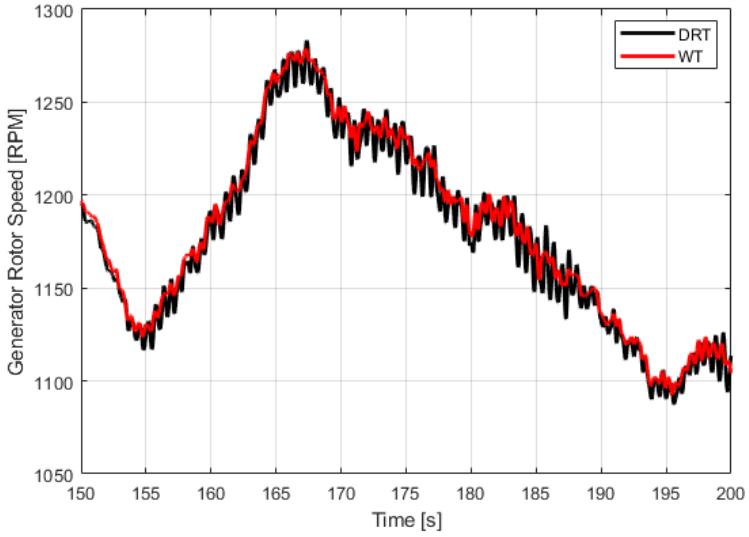

Figure 3.15: Generator speed response during 18 m/s turbulent wind for coupled detailed nacelle-test bench with tuned PI controller (DRT) model vs. nacelle coupled to flexible rotor (WT) in time domain.

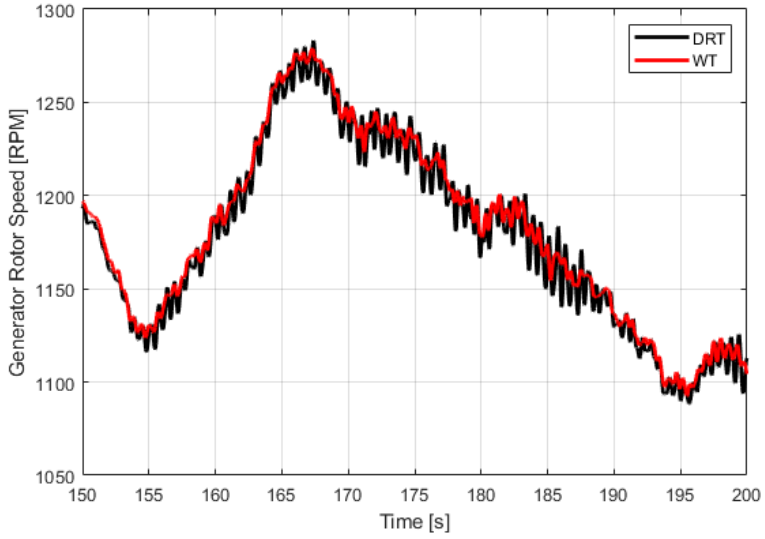

Figure 3.16: Generator speed response during 18 m/s turbulent wind for coupled detailed nacelle-test bench with tuned PID controller (DRT) model vs. nacelle coupled to flexible rotor (WT) in time domain.

These results suggest considering gain-scheduling approach wherein different sets of gains can be utilized depending on the nature of the test (free versus forced response) if better tracking performance is desired. As an example, while not optimized, repeating the previous simulation

with lower PI controller gains lowers the amplitude of torsional oscillations leading to reduced RMS tracking error of 5.6 RPM. The resulting generator speed responses for this case are shown in Fig. 3.17.

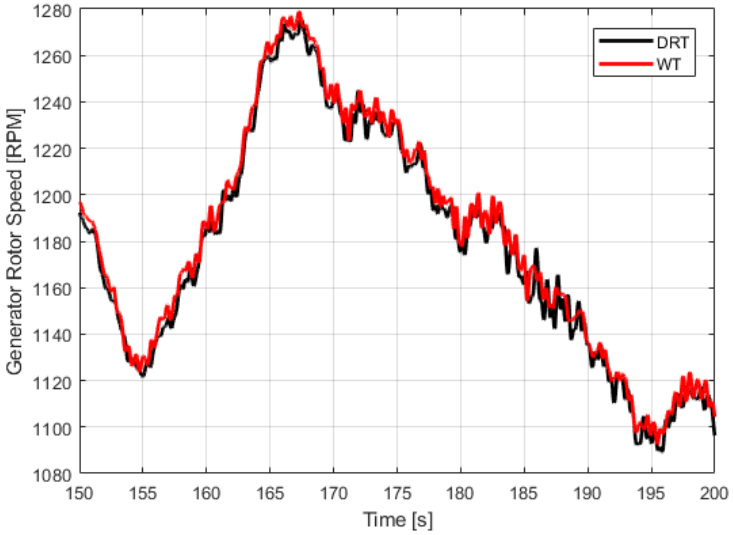

Figure 3.17: Generator speed response during 18 m/s turbulent wind for coupled detailed nacelle-test bench model with lower PI controller gains (DRT) vs. nacelle coupled to flexible rotor (WT) in time domain.

Chapter 4

Conclusions

Chapter 2 considers modeling aspects of developing a Hardware-In-the-Loop setup for testing full-scale offshore wind turbine nacelles. First, a simulation based analysis is performed to study the influence of varying the fidelity of various components within the drivetrain on the turbine's dynamic responses. This analysis provides an understanding of the modeling requirements that will result in acceptable real-time performance while capturing the dynamics of drivetrain components accurately with focus on torsional responses necessary to perform electro-mechanical certification tests with the HIL setup. For the case study considered in this analysis, it is shown that the flexibility of the main shaft and gearbox supports are the main parameters to capture the torsional response accurately. The other structural elements such as gearbox housing and bedplate have negligible influence and hence can be modeled as rigid elements. Additionally, the components within the gearbox can be simplified by considering only the rotational degree of freedom without accounting for advanced gear pair interactions.

Next, an analysis is performed to characterize the influence of the differences in boundary conditions between the nacelle mounted on the test bench and the nacelle model running in parallel within the full turbine real-time simulation. A free response analysis showed the abstracted nacelle on the test bench exhibits a higher torsional frequency when compared to the full turbine due to the missing rotor. Furthermore, forced response analysis showed that the dynamic responses of several components within the drivetrain in the abstracted nacelle can be significantly different with higher frequency content when compared to the those from the full turbine. This is mainly driven by the missing platform and tower which act as a low-pass filter.

In Chapter 3, a method of tuning the test bench speed controller is explored to match the torsional behavior of the nacelle on a test bench to a nacelle in the field. First, a simple 3-DOF closed-loop system is introduced with a speed controller to investigate the feasibility of using pole placement to emulate the torsional modes of a full wind turbine on the test bench. The symbolic state space matrices are first derived for the closed-loop system with a PI controller. An iterative approach is used to generate several root loci corresponding to the parameter space represented by the different ranges of the controller gains. The root locus that is closest to/passing through the desired poles is identified. The corresponding proportional and integral gains are selected so that the first torsional mode of the closed-loop system matches the turbine mode as in the field. The closed-loop system is then evaluated with a PID controller. It is demonstrated that the controller can be tuned to match the first and second torsional modes successfully. The pole placement technique is then applied to a high-fidelity representation of the test bench-nacelle model consisting of 45 dynamic states. It is illustrated through a free and forced response evaluation that tuning the test bench speed controller can effectively eliminate variations due to boundary conditions and better replicate transient field events on the test bench. This enables the development of a Hardware-In-the-Loop testing platform to allow for full turbine operational testing with the native nacelle controller and to perform more realistic electro-mechanical certification tests.

Bibliography

[1] Global wind energy council: Global wind report 2019, February 2020.

[2] A. Greco, S. Sheng, J. Keller, and A. Erdemir. Condition indicators for gearbox condition monitoring systems. *Wear*, 302(6):1583–1591, 2013.

[3] F. D. Coninck, W. Desmet, P. Sas, J. Peeters, Rob Huijskens, and Dirk Leimann. Reproduction of dynamic load cases on a 13.2 mw test facility for wind turbine gearboxes. 2010.

[4] Andrea Montecucco, James Buckle, Jonathan Siviter, and Andrew Knox. A new test rig for accurate nonparametric measurement and characterization of thermoelectric generators. *Journal of Electronic Materials*, 42:1–8, 07 2013.

[5] Jongmin Cheon, Jinwook Kim, Joohoon Lee, Kichang Lee, and Youngkiu Choi. Development of hardware-in-the-loop-simulation testbed for pitch control system performance test. *Energies*, 12:2031, 05 2019.

[6] Jessica Holierhoek, Denja Lekou, T. Hecquet, H. Söker, B. Ehlers, Feike Savenije, Wouter Engels, R.P. Pieterman, M. Ristow, M. Kochmann, Kris Smolders, and Joris Peeters. Procedures for testing and measuring wind turbine components; results for yaw and pitch system and drive train. *Wind Energy*, 16, 09 2013.

[7] IEC 61400-21: Wind turbines – Part 1: Design requirements.

[8] IEC 61400-21: Wind turbines – Part 21: Measurement and assessment of power quality characteristics of grid connected wind turbines.

[9] Alexander Helmedag, Timo Isermann, Uwe Jassmann, Dominik Radner, Dirk Abel, Georg Jacobs, and Antonello Monti. Testing nacelles of wind turbines with a hardware in the loop test bench. *IEEE Instrumentation & Measurement Magazine*, 17(5):26–33, 2014.

[10] J. Jonkman and M. Buhl Jr. *FAST User's Guide*. NREL, Golden, Colorado, 2005.

[11] J. Jonkman and L. Kilcher. *TurbSim User's Guide: Version 1.06.00*. NREL, Golden, Colorado, 2012.

[12] J. Jonkman, S. Butterfield, W. Musial, and G. Scott. Definition of a 5-MW reference wind turbine for offshore system development. Technical Report NREL/TP-500-38060, National Renewable Energy Laboratory, Golden, Colorado, February 2009.

[13] Nathaniel Beasley. Effects of component model fidelity level on dynamic analysis accuracy of a multi-mw wind turbine drivetrain. Master's thesis, Clemson University, 2019.

[14] Ryan Schkoda and Amin Bibo. A hardware-in-the-loop strategy for control of a wind turbine test bench. page V002T21A003, 10 2015.

[15] R. Schkoda, A. Bibo, Y.Guo, S. Lambert, and R. Wallen. Characterizing the influence of abstraction in full-scale wind turbine nacelle testing. volume 8: 28th Conference on Mechanical Vibration and Noise of *International Design Engineering Technical Conferences and Computers and Information in Engineering Conference*, 08 2016. V008T10A010.

[16] Berthold Schlecht, Thomas Rosenlöcher, and Georg Breslau. Possibilities and limitations of the load determination for wind turbines using the multibody-system simulation. In *Conference for Wind Power Drives 2017: Tagungsband zur Konferenz*, volume 3, page 227. BoD–Books on Demand, 2017.

[17] Kirk Heinold, Amin Bibo, and Meghashyam Panyam. Modeling considerations for testing full-scale off-shore wind turbine nacelles with hardware-in-the-loop. In *Proceedings of the ASME 2020 International Design Engineering Technical Conferences and Computers and Information in Engineering Conference*, St. Louis, MO, 2020. ASME.

[18] Kirk Heinold, Amin Bibo, and Meghashyam Panyam. Considerations for testing full-scale wind turbine nacelles with hardware-in-the-loop. In *Forsch Ingenieurwes*, 2021.

[19] U. Jassman. *Hardware-in-the-Loop Wind Turbine System Test Benches and their Usage for Controller Validation.* PhD thesis, RWTH Aachen University, 2018.